AHEAD OF PRINT

Original papers

Angiology; cardiology; heart and cardiovascular system

Machine learning identifies autophagy biomarkers driving microvascular injury in cardiac ischemia/reperfusion

Lina Tan[1,3,A–F], Jingjing Rao[1,3,B,C], Yue Wang[1,3,A,C], Liangbo Hu[1,3,B,C], Min He[1,3,B,C], Jinyuan Tan[1,B,C], Xiaocong Zeng[2,3,A,E,F]

[1] Department of Cardiology, The First Affiliated Hospital of Guangxi Medical University, Nanning, China

[2] 1st Department of Cardiology, The First Affiliated Hospital of Guangxi Medical University, Nanning, China

[3] Guangxi Key Laboratory Base of Precision Medicine in Cardiocerebrovascular Diseases Control and Prevention Guangxi Clinical Research Center for Cardio-Cerebrovascular Diseases, Nanning, China

A – research concept and design; B – collection and/or assembly of data; C – data analysis and interpretation; D – writing the article; E – critical revision of the article; F – final approval of the article

Advances in Clinical and Experimental Medicine, ISSN 1899–5276 (print), ISSN 2451–2680 (online) *Adv Clin Exp Med*. 2026

Address for correspondence
Xiaocong Zeng
E-mail: aban829@163.com

Funding sources
National Natural Science Foundation of China (grant No. 82260069).

Conflict of interest
None declared

Received on June 27, 2025
Reviewed on October 1, 2025
Accepted on November 21, 2025

Published online on September 17, 2026

Abstract

Background. Ischemic heart disease (IHD) remains a leading global cause of mortality. While reperfusion is essential for treating ischemic cardiomyopathy, it paradoxically induces myocardial ischemia/reperfusion (I/R) injury targeting the microvascular endothelium. The link between autophagy and microvascular damage in myocardial I/R requires clarification.

Objectives. This study aimed to identify autophagy-related biomarkers of myocardial I/R injury using integrated bioinformatics and experimental validation, characterize the associated molecular and immune features, and evaluate the role of Myc in cardiac microvascular endothelial injury.

Materials and methods. Bioinformatics analysis of Gene Expression Omnibus (GEO) multi-chip datasets intersected autophagy-related genes (HADb) with differentially expressed genes (DEGs) to identify signature biomarkers using machine-learning algorithms. Diagnostic efficacy was validated using a nomogram. Mechanistic exploration through gene set enrichment analysis (GSEA) and immune profiling revealed I/R subtypes. Biomarker expression was externally validated in the GSE168610 dataset. Myocardial I/R models were assessed using echocardiography (cardiac function), Evans blue/TTC staining (infarction area), and ink perfusion (microvascular density). Hub gene expression was quantified using quantitative polymerase chain reaction (qPCR), western blot (WB), and immunohistochemistry (IHC). In vitro, c-Myc-knockout cardiac endothelial cells underwent hypoxia/reoxygenation (H/R), followed by analysis of autophagy (WB), apoptosis (TUNEL), and autophagic vacuoles (transmission electron microscopy (TEM)).

Results. Seven autophagy-related DEGs were identified and linked to muscle proliferation, protease activation, and oncogenesis. Four signature genes (*Casp4*, *Cdkn1a*, *Myc*, and *Rgs19*) were identified by 3 machine-learning algorithms, with diagnostic validation. In the development cohort, the AUCs ranged from 0.756 to 0.876. In the external-validation cohort, the AUC was 1.000 for Casp4, Myc, and Rgs19 and 0.875 for Cdkn1a. GSEA linked these genes to tricarboxylic acid cycle (TCA) dysregulation and immune infiltration. Unsupervised clustering identified 2 molecular subtypes. C1 exhibited higher expression of 6 of the 7 autophagy-related DEGs, whereas C2 showed higher proportions of mast cells and activated dendritic cells and enrichment of mitochondrial and energy-metabolism pathways. c-Myc knockout reduced endothelial apoptosis and autophagic injury.

Conclusions. c-*Myc* emerged as a critical driver linking excessive autophagy to microvascular damage, providing a promising diagnostic and therapeutic target for reperfusion injury management.

Key words: autophagy, biomarkers, myocardial ischemia, reperfusion injury, microcirculation

Cite as
Tan L, Rao J, Wang Y, et al. Machine learning identifies autophagy biomarkers driving microvascular injury in cardiac ischemia/reperfusion [published online as ahead of print on September 17, 2026]. *Adv Clin Exp Med*. 2026. doi:10.17219/acem/214581

DOI
10.17219/acem/214581

Highlights

- In the development cohort, the AUCs ranged from 0.756 to 0.876; in the external-validation cohort, the AUCs ranged from 0.875 to 1.000.
- The study demonstrates that c-Myc is a critical regulator connecting excessive autophagy with microvascular endothelial injury during myocardial reperfusion, positioning it as a potential therapeutic target.
- Unsupervised clustering identified 2 molecular subtypes. C1 showed higher expression of 6 of the 7 autophagy-related DEGs and greater M0 macrophage infiltration, whereas C2 showed higher proportions of mast cells and activated dendritic cells and enrichment of mitochondrial and energy-metabolism pathways.
- Biomarker expression was validated in external datasets and I/R models using qPCR, Western blot, and immunohistochemistry, confirming their association with cardiac dysfunction, infarct size, and microvascular density.

Background

Ischemic heart disease (IHD) remains one of the leading causes of mortality worldwide, with both its prevalence and mortality increasing substantially on a global scale.[1] Over the past 3 decades, the incidence and mortality of IHD have increased by 103.5% and 60.4%, respectively, and are projected to continue rising over the next 2 decades.[2] Although early reperfusion remains the cornerstone of treatment for ischemic cardiomyopathy, it can paradoxically induce ischemia/reperfusion (I/R) injury. Myocardial I/R injury is characterized by tissue damage resulting from insufficient blood supply during ischemia, which is exacerbated upon reperfusion.[3] The pathological manifestations of myocardial I/R include myocardial stunning, the no-reflow phenomenon, reperfusion arrhythmias, and lethal reperfusion injury.[4] The no-reflow phenomenon, driven by microvascular injury, is a fundamental mechanism of myocardial I/R injury and an independent predictor of mortality and recurrent myocardial infarction.[5,6] Compared with cardiomyocytes, cardiac microvascular endothelial cells sustain earlier and more severe injury during myocardial I/R.[7] This injury is closely associated with several pathogenic mechanisms, including calcium overload,[8] endoplasmic reticulum stress,[9] mitochondrial dysfunction, and impaired mitochondrial quality control.[10,11] Despite extensive research aimed at elucidating the mechanisms underlying myocardial I/R-induced microvascular injury and developing novel therapeutic strategies, early diagnosis, timely intervention, and a comprehensive understanding of the underlying mechanisms remain major challenges.

With increasing insight into the pathophysiological mechanisms of microvascular injury during myocardial I/R, autophagy has emerged as a promising therapeutic target. Autophagy, a fundamental intracellular degradation and recycling process, plays an essential role in cardiovascular homeostasis by removing damaged mitochondria and protein aggregates.[12] While physiological levels of autophagy support cellular homeostasis, excessive activation may lead to cellular dysfunction and death.[13] Accumulating evidence has linked dysregulated autophagy to the initiation and progression of microvascular injury during myocardial I/R. Cardiac microvascular endothelial cells, which account for more than 60% of the total cardiac cell population, possess a tightly regulated autophagic system. Impaired autophagy can compromise endothelial cell integrity.[14] Experimental models of myocardial I/R have demonstrated excessive autophagy in cardiac microvascular endothelial cells and have shown that inhibition of autophagy attenuates cellular injury and apoptosis.[15,16] Conversely, autophagy activation has also been reported to exert protective effects against myocardial I/R injury, highlighting its dual role in the I/R process.[17] Therefore, a comprehensive evaluation of autophagy may improve our understanding of the molecular mechanisms underlying the no-reflow phenomenon associated with microvascular I/R injury and facilitate the identification of potential diagnostic biomarkers.

Objectives

Despite advances in cardiac I/R research at the genomic level, studies specifically investigating autophagy-related genes in the context of myocardial I/R-induced microvascular injury remain limited. This gap hinders a comprehensive understanding of the underlying molecular mechanisms and the identification of potential diagnostic biomarkers. Therefore, the present study was designed to identify and characterize key autophagy-related genes associated with microvascular injury during myocardial I/R.

This study aimed to identify novel biomarkers for the diagnosis of myocardial I/R injury by integrating bioinformatics and experimental validation. It also investigated the functional role of dysregulated autophagy in microvascular injury, identified key biomarkers, and explored the mechanistic link between autophagy, microvascular injury, and the regulator *c-Myc*.

Materials and methods

Microarray data retrieval and pre-processing

Cardiac I/R datasets were retrieved from the National Center for Biotechnology Information (NCBI) Gene Expression Omnibus (GEO) database (http://www.ncbi.nlm.nih.gov/geo) using the keywords "myocardial ischemia/reperfusion injury" and "cardiac ischemia/reperfusion injury". Seven datasets (GSE108940, GSE115568, GSE4105, GSE58486, GSE61592, GSE83472, and GSE168610) were retrieved from the GEO database on June 5, 2024. A combined multi-chip cohort comprising 25 sham samples and 28 I/R samples from GSE108940, GSE115568, GSE4105, GSE58486, GSE61592, and GSE83472 (Supplementary Table 1) underwent batch-effect correction using the SVA R package (https://www.bioconductor.org/packages//release/bioc/html/sva.html). The effectiveness of batch correction was assessed using principal component analysis (PCA) plots generated with the ggplot2 package (https://cran.r-project.org/web/packages/ggplot2/index.html). The first 6 datasets were used to identify differentially expressed genes (DEGs), whereas GSE168610 was used for external validation.

DEGs identification

Differential expression analysis between the sham and I/R groups was performed using the limma R package (https://bioconductor.org/packages/release/bioc/html/limma.html). Heatmaps and volcano plots were generated using the pheatmap (https://cran.r-project.org/web/packages/pheatmap/index.html) and ggplot2 packages. Genes with a $p < 0.05$ and an absolute log₂ fold change (|log₂FC|) >1.0 were considered DEGs. The top 20 DEGs were visualized in a heatmap.

Identification of DEGs related to autophagy and functional enrichment analysis

A total of 215 autophagy-related genes (ARGs) were retrieved from the Human Autophagy Database (HADb; http://autophagy.lu) and converted to their mouse homologs. Differentially expressed autophagy-related genes (ARDEGs) were identified using Venn diagram analysis by intersecting the DEGs with the ARGs. Functional enrichment analysis of ARDEGs was performed using Gene Ontology (GO) (http://geneontology.org) analysis (biological process (BP), cellular component (CC), and molecular function (MF)) and Kyoto Encyclopedia of Genes and Genomes (KEGG) (https://www.kegg.jp) pathway analysis (ClusterProfiler; https://bioconductor.org/packages/release/bioc/html/clusterProfiler.html). Results with a $p < 0.05$ were visualized as bubble plots using ggplot2.

Recognition of hub genes based on well-established machine learning algorithms

Machine-learning algorithms – including least absolute shrinkage and selection operator (LASSO; glmnet R package (https://cran.r-project.org/web/packages/glmnet/index.html)), support vector machine–recursive feature elimination (SVM-RFE; e1071/MSVM-RFE), and Random Forest (RF; randomForest (https://cran.r-project.org/web/packages/randomForest/index.html)) – were used to identify signature genes associated with cardiac microvascular I/R injury. Using the 7 shared ARDEGs as input, LASSO with 10-fold cross-validation was applied to calculate regression coefficients and identify the optimal features based on partial likelihood deviance and λ-logarithm curves (cv.glmnet; https://www.rdocumentation.org/packages/glmnet/versions/5.0/topics/cv.glmnet). SVM-RFE performed sequential backward feature selection to identify key hub genes at the highest 5-fold cross-validation accuracy (highlighted by a red circle). Random Forest ranked gene importance using an ensemble of decision trees. Hub genes were defined as those identified by all 3 machine-learning algorithms, as illustrated in the Venn diagram.

Nomogram construction and ROC evaluation

To further evaluate the predictive performance of the model, a nomogram was constructed by integrating the 4 hub genes using the rms package (https://cran.r-project.org/web/packages/rms/index.html) in R. A score was assigned to the expression level of each gene, and the total score was used to estimate the probability of I/R injury. Model performance was evaluated using decision curve analysis (DCA) and calibration curves. In addition, the area under the receiver operating characteristic (ROC) curve (AUC) was calculated to assess the diagnostic performance of each candidate biomarker.

Single-gene gene set enrichment analysis

Single-gene gene set enrichment analysis (GSEA) of the 4 diagnostic genes was performed using the ClusterProfiler package. To investigate the association between the underlying molecular mechanisms and gene expression phenotypes, Hallmark gene sets were retrieved from the Molecular Signatures Database (MSigDB; version accessed May 18, 2024) (https://www.gsea-msigdb.org/gsea/msigdb/mouse/genesets.jsp?collection=MH). Enrichment plots were generated to display the top 5 positively and negatively enriched pathways for each gene in the 2 study groups.

Immune cell infiltration analysis

The CIBERSORT R package (https://github.com/Moonerss/CIBERSORT) was used to estimate the relative

proportions of immune cell populations in the combined multi-chip datasets from the I/R and sham groups. Based on gene expression data, the CIBERSORT algorithm was applied to estimate immune cell abundance by deconvolution, and the results were visualized as bar plots. In addition, the ggplot2 package was used to generate lollipop plots illustrating the correlations between the expression of each hub gene and immune cell abundance.

Unsupervised clustering analysis of I/R subtypes

Ischemia/reperfusion subtypes were identified using consensus clustering with the ConsensusClusterPlus R package (https://www.rdocumentation.org/packages/ConsensusClusterPlus/versions/1.36.0/topics/ConsensusClusterPlus) based on the expression profiles of AR-DEGs (1,000 iterations). The optimal number of clusters was determined using the consensus matrix, cumulative distribution function (CDF) index, and the relative change in the area under the CDF curve. Intercluster heterogeneity was assessed using PCA and box plots. Functional differences, including immune cell infiltration and KEGG/GO pathway enrichment, were compared between Cluster 1 and Cluster 2.

Validation of hub genes within the dataset

The GSE168610 dataset served as an external validation cohort. Raw data retrieved from the GEO database underwent expression matrix transformation using Perl and normalization with the limma R package. Expression levels of the 4 hub genes were extracted, compared between groups using the Wilcoxon rank-sum test, and visualized as violin plots. Diagnostic performance was evaluated using receiver operating characteristic (ROC) curves, and the area under the curve (AUC) was calculated for each biomarker.

Animals

A total of 60 healthy adult male C57BL/6J mice (8–10 weeks old, 18–22 g) were obtained from the Guangxi Medical University Laboratory Animal Center (Nanning, China). The mice were housed at 21–23°C with a relative humidity of 55 ±5%. Before the experiments, they had ad libitum access to food and water and were maintained under a 12-h light/dark cycle. The animal facility was cleaned regularly to maintain standardized housing conditions. All animal experiments were conducted in accordance with the applicable Chinese regulations and were approved by the Animal Ethics Committee of Guangxi Medical University (approval No. 202401020).

Myocardial I/R model establishment and electrocardiogram and echocardiography analysis

Mice were randomly assigned to the sham (n = 30) or I/R (n = 30) group using a lottery-drawing method. Anesthesia was induced by intraperitoneal administration of avertin (1.25%, 0.2 mL/10 g). Myocardial ischemia/reperfusion was induced by 45 min of left anterior descending coronary artery (LAD) ligation using an 8-0 silk suture, followed by 120 min of reperfusion.[18,19] Sham-operated mice underwent the same surgical procedure without LAD ligation. Cardiac function was assessed after reperfusion using a VINNO D700 VET ultrasound system under 1–2% isoflurane anesthesia. Left ventricular ejection fraction (LVEF) and left ventricular fractional shortening (LVFS) were measured using B-mode and M-mode imaging over 3 consecutive cardiac cycles. Electrocardiography (ECG) was performed before ischemia and after reperfusion using an ECG-3306G system (Sanyue, Guangzhou, China).

Subsequently, mice designated for Evans blue/TTC staining (n = 16) and gelatin–ink perfusion (n = 16) underwent intracardiac perfusion with the respective solutions under continuous anesthesia before heart excision. Mice assigned to the tissue analysis cohort (n = 12) and the molecular analysis cohort (n = 16) were euthanized by anesthetic overdose, and the hearts were immediately harvested and snap-frozen at −80°C. All subjectively assessed outcomes (specifically histological scoring, infarct size analysis, and behavioral video analysis) were evaluated by an independent investigator blinded to the experimental group assignments.

Evans blue and TCC staining analysis

After 120 min of reperfusion, myocardial infarct size was assessed using 2,3,5-triphenyltetrazolium chloride (TTC) and Evans blue staining. A 2% Evans blue solution was retrogradely perfused through the right ventricle until cyanosis of the extremities was observed. Hearts were excised, rinsed with saline, frozen at −20°C for 10 min, and sectioned into 1-mm-thick slices. The sections were incubated in the dark with 1% TTC (Leagene Biotechnology, Anhui, China) at 37°C for 30 min. Infarct size was quantified as the proportion of white ischemic tissue relative to the total left ventricular area using ImageJ (National Institutes of Health (NIH), Bethesda, USA).

Gelatin-ink perfusion

Following 120 min of reperfusion, hearts were perfused through the right ventricle with 4% gelatin–ink to achieve uniform cardiac staining. The tissues were harvested, fixed in 4% paraformaldehyde, and sectioned. Microvascular architecture was examined at ×20 magnification using an Olympus BX53 light microscope (Olympus Corp., Tokyo, Japan), and images were acquired for quantitative morphometric analysis.

Immunohistochemical staining

Cardiac tissues were fixed in 4% paraformaldehyde, embedded in paraffin, and sectioned at a thickness of 5 μm. After deparaffinization and antigen retrieval, endogenous peroxidase activity was blocked with 3% H_2O_2, followed by blocking with 3% bovine serum albumin (BSA) at room temperature for 30 min. Sections were incubated overnight at 4°C with anti-c-Myc (1:200; HA721182; Huabio, Hangzhou, China) or anti-caspase-4 (1:300; ER60011; Huabio) primary antibodies, followed by incubation with horseradish peroxidase (HRP)-conjugated secondary antibodies. 3,3′-Diaminobenzidine (DAB) was used as the chromogenic substrate, followed by hematoxylin counterstaining. Images were acquired using an Olympus BX53 light microscope, and positively stained areas were quantified using ImageJ.

Cell culture and hypoxia/reoxygenation model

Cardiac microvascular endothelial cells (CMECs) were obtained from Procell Life Science (cat. No. CP-M129; Procell, Wuhan, China). Quality control confirmed CD31 immunofluorescence positivity ≥90%, the absence of HIV-1, HBV, HCV, and mycoplasma (polymerase chain reaction (PCR)-tested), and the absence of microbial contamination (culture-verified). Cells were cultured in mouse cardiac microvascular endothelial cell complete medium (ECM; cat. No. CM-M129; Procell) at 37°C in a humidified atmosphere containing 5% CO_2. At 80–90% confluence, CMECs between passages 3 and 8 were subjected to hypoxia in glucose- and fetal bovine serum (FBS)-free Dulbecco's modified Eagle's medium (DMEM; cat. No. PM150122; Procell) under 1% O_2, 5% CO_2, and 94% N_2 for 24 h, followed by reoxygenation in complete medium under 95% O_2 and 5% CO_2 for 24 h.

siRNA transfection

Cells were seeded and cultured for 24 h to achieve 70–80% confluence before transfection with siRNA targeting *Myc* (*si-Myc*) (sequence: TGGAGATGATGACCGAGTTAC; Hanbio Co., Ltd., Shanghai, China) using Lipo8000™ transfection reagent (C0533; Beyotime Biotechnology, Shanghai, China). The transfection complex was prepared by mixing the siRNA with Lipo8000™ in antibiotic- and serum-free DMEM, followed by incubation at room temperature for 20 min. The transfection complex was then added to the CMEC culture and incubated for 24 h. Subsequently, the transfection medium was replaced with glucose- and serum-free DMEM, and the cells were subjected to 24 h of hypoxia followed by 24 h of reoxygenation.

TUNEL staining assay

To evaluate apoptosis in CMECs in vitro, a terminal deoxynucleotidyl transferase-mediated dUTP nick-end labeling (TUNEL) assay kit (Beyotime Biotechnology) was used. After hypoxia/reoxygenation (H/R) treatment, CMECs at an appropriate density were selected for TUNEL staining. According to the manufacturer's instructions, the cells were washed, fixed, permeabilized, and incubated with the TUNEL reaction mixture at 37°C in the dark. Images were acquired using a fluorescence microscope (200× magnification; Zeiss Axiocam 506 Color; Carl Zeiss AG, Jena, Germany).

Transmission electron microscopy of mitochondria

Cell pellets (1×10^7 cells) were fixed in 2.5% glutaraldehyde at 4°C for 24 h, rinsed with phosphate-buffered saline (PBS), and post-fixed in 1% osmium tetroxide for 2 h. En bloc staining was performed with uranyl acetate in 70% ethanol for 3 h. After graded ethanol dehydration, samples were treated with propylene oxide, infiltrated with Eponate 12 resin (hardener: DDSA/NMA/DMP-30), and polymerized at 45°C for 12 h, followed by 72°C for 24 h. Ultrathin sections (70 nm) were prepared using a Leica UC-7 ultramicrotome (Leica Camera AG, Wetzlar, Germany), stained with lead citrate, and examined using a JEOL JEM-1400 transmission electron microscope (TEM) (80 kV; Morada G3 CCD; JEOL Ltd., Tokyo, Japan). Mitophagy was identified by the presence of double-membrane autophagosomes containing mitochondria with disrupted cristae.

RT-qPCR assay

Total RNA was isolated from myocardial tissues and cultured cells using TRIzol reagent (Solarbio, Beijing, China). RNA concentration and purity (A260/A280 ratio) were measured using a NanoDrop spectrophotometer (Thermo Fisher Scientific, Waltham, USA). Complementary DNA (cDNA) was synthesized from 1,000 ng of RNA using HyperScript III RT SuperMix (R202; EnzyArtisan Biotech, Shanghai, China). Quantitative reverse transcription polymerase chain reaction (RT-qPCR) was performed using ×2 S6 Universal SYBR Mix (Q204-1; EnzyArtisan Biotech) on a 7500 Real-Time PCR System (Thermo Fisher Scientific). Primer sequences are listed in Supplementary Table 2. The thermal cycling conditions were as follows: 95°C for 10 min, followed by 40 cycles of 95°C for 15 s, 60°C for 30 s, and 72°C for 30 s. For RT-qPCR, 5 independent myocardial tissue samples per group and 6 independent cell samples per group were analyzed. Each RNA sample was measured in 3 technical replicates, and the technical-replicate Ct values were averaged before downstream analysis. Gene expression levels were normalized to GAPDH and calculated using the $2^{-\Delta\Delta Ct}$ method.

Western blot assay

Cardiac tissues were homogenized in radioimmunoprecipitation assay (RIPA) buffer (R0010; Solarbio) containing protease and phosphatase inhibitors (P1261; Solarbio). Protein concentration was determined using a bicinchoninic acid (BCA) assay kit (P0398S; Beyotime Biotechnology) at 562 nm. Equal amounts of protein (20 μg/lane) were separated by 10% sodium dodecyl sulfate-polyacrylamide gel electrophoresis (SDS-PAGE), transferred to polyvinylidene difluoride (PVDF) membranes (ISEQ00010; MilliporeSigma, St. Louis, USA), and blocked with 5% non-fat milk in Tris-buffered saline with Tween-20 (TBST) for 2 h at room temperature. Membranes were incubated overnight at 4°C with the following primary antibodies: anti-caspase-4 (1:500; TA5130; Abmart, Shanghai, China), anti-c-Myc (1:1,000; T55150; Abmart), anti-Cdkn1a (1:1,000; #382492; Zen-Bioscience, Chengdu, China), anti-Bax (1:1,000; #50599-2-Ig; Proteintech, Wuhan, China), anti-Bcl-2 (1:1,000; #26593-1-AP; Proteintech), anti-LC3 (1:1,000; #382687; Zen-Bioscience), anti-GAPDH (1:10,000; #301341; Zen-Bioscience), and anti-β-tubulin (1:5,000; #48375; Signalway Antibody, USA). After washing with TBST, HRP-conjugated secondary antibodies (1:10,000; #301341; Zen-Bioscience) were applied for 1 h at room temperature. Protein bands were visualized using an e-BLOT Touch Imager (Ebiotrade Life Science, Shanghai, China) and quantified using ImageJ.

Statistical analyses

All bioinformatics and statistical analyses were performed using R v. 4.3.3 (R Foundation for Statistical Computing, Vienna, Austria). Statistical analyses and graphical visualizations were generated using GraphPad Prism v. 8.0 (GraphPad Software, San Diego, USA). All statistical analyses were performed in accordance with the statistical guidelines of *Advances in Clinical and Experimental Medicine*.[20] The results of all assumption checks for parametric tests are presented in Supplementary Table 5.

The normality of data distribution was assessed using the Shapiro–Wilk test. Data are presented as the mean ± standard deviation (SD) for normally distributed variables or as the median with the 1st and 3rd quartiles (Q1 and Q3) for non-normally distributed variables. Differences between 2 independent groups were analyzed using the Mann–Whitney U test. Comparisons among multiple groups were performed using one-way analysis of variance (ANOVA) followed by Tukey's post hoc test. A $p < 0.05$ was considered statistically significant.

Results

Identification of DEGs

After batch-effect correction, PCA demonstrated a more homogeneous distribution of samples across all datasets (Fig. 1A). A total of 402 DEGs were identified across the 6 datasets, including 168 downregulated and 234 upregulated genes, using the thresholds of $p < 0.05$ and an absolute log₂ fold change (|log₂FC|) >1.0 (Fig. 1B). A clustered heatmap further illustrates the expression profiles of the top 20 DEGs in the 2 study groups (Fig. 1C).

Functional enrichment analysis of ARDEGs

The Venn diagram in Fig. 2A shows that 7 genes were identified at the intersection of the DEGs and ARGs. These 7 genes (*Casp4*, *Cdkn1a*, *Edem1*, *Egfr*, *Hif1a*, *Myc*, and *Rgs19*) were significantly upregulated in the I/R group compared with the sham group (Fig. 2B). To gain further functional insight, GO enrichment analysis was performed to characterize the BP, CC, and MF associated with the ARDEGs. As shown in Fig. 2C, the ARDEGs were significantly enriched in several biological processes, including the regulation of smooth muscle cell proliferation, positive regulation of microRNA (miRNA) metabolic processes, and regulation of miRNA transcription. With respect to cellular components, the ARDEGs were significantly associated with euchromatin, RNA polymerase II transcription regulator complexes, and membrane rafts. Molecular function analysis identified significant enrichment for ubiquitin or ubiquitin-like protein ligase binding, E-box binding, and protein kinase activator activity. Furthermore, KEGG pathway analysis demonstrated significant enrichment in pathways including proteoglycans in cancer, bladder cancer, the ErbB signaling pathway, the HIF-1 signaling pathway, hepatitis C, and the JAK-STAT signaling pathway (Fig. 2D).

Identification of the hub genes via machine learning algorithms

Based on the 7 shared genes, 3 machine-learning algorithms – LASSO, SVM-RFE, and RF – were used to identify the most promising candidate biomarker genes. The LASSO coefficient path plot identified 7 genes with nonzero regression coefficients. Using 10-fold cross-validation, the optimal λ value corresponding to the minimum cross-validation error was selected, resulting in the identification of 6 key feature genes (Fig. 3A). The performance of the SVM-RFE model was evaluated using 5-fold cross-validation, leading to the identification

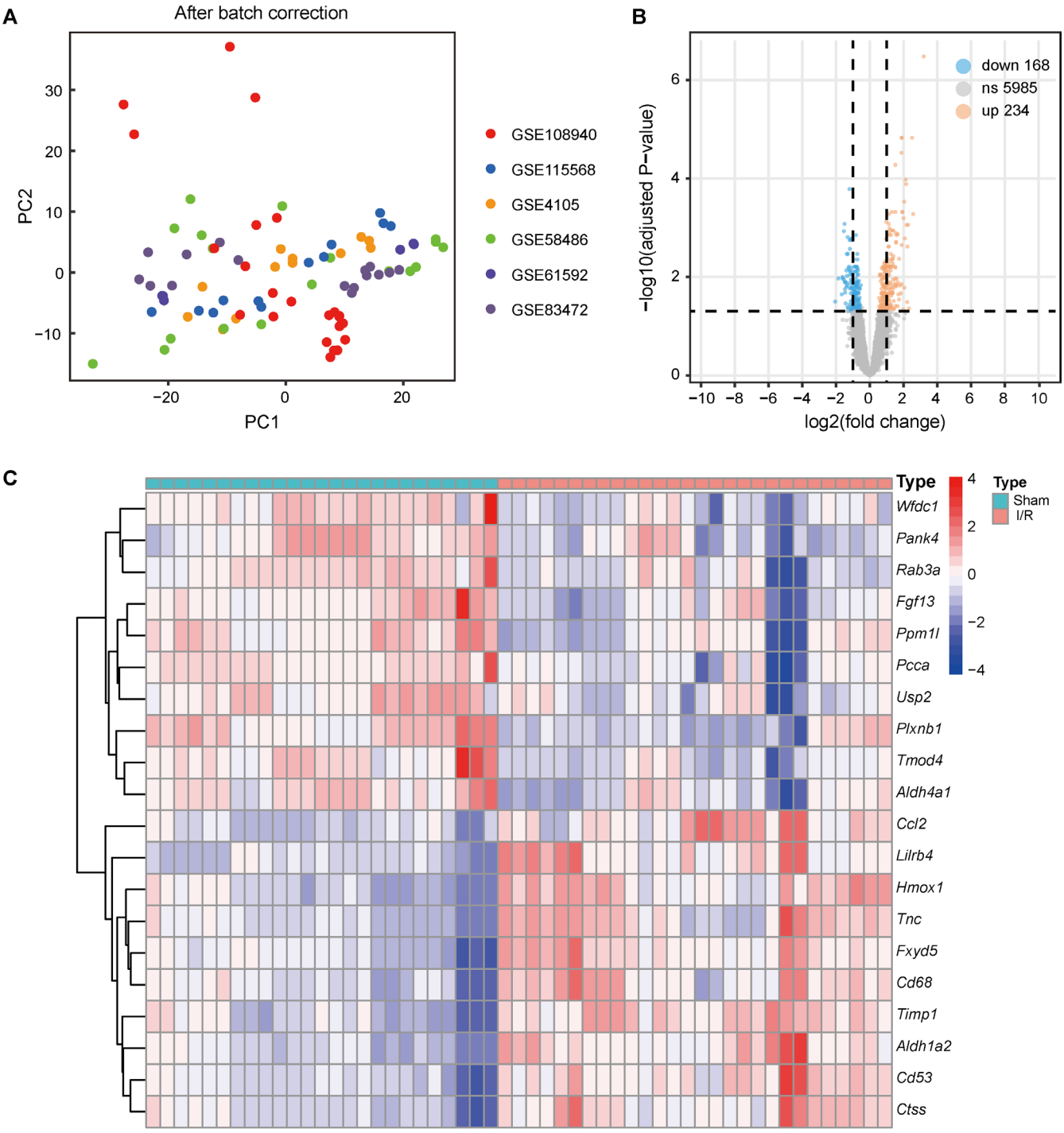

Fig. 1. Identification of differentially expressed genes (DEGs) associated with myocardial ischemia/reperfusion (I/R). A. Principal component analysis (PCA) plot showing gene expression profiles after batch-effect correction; B. Volcano plot showing DEGs between the sham and I/R groups; C. Heatmap showing the top 20 DEGs between the 2 groups

of 6 key genes with the lowest error rate and highest classification accuracy (Fig. 3B). Subsequently, the RF algorithm identified 7 genes with importance scores >2.0 as potential biomarkers for I/R injury (Fig. 3C). Ultimately, 4 hub genes (*Casp4*, *Cdkn1a*, *Myc*, and *Rgs19*) were consistently identified by all 3 algorithms, as illustrated in the Venn diagram (Fig. 3D).

Evaluation of diagnostic efficacy for hub biomarkers via nomogram

To further evaluate the predictive performance for myocardial I/R injury, a nomogram was constructed using the 4 candidate hub biomarkers (*Casp4*, *Cdkn1a*, *Myc*, and *Rgs19*), providing a simple and reliable diagnostic

A

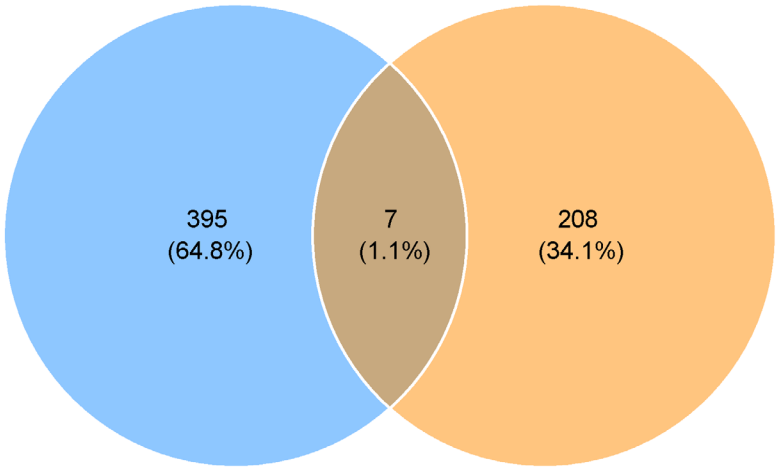

B

Gene	Gene description	I/R vs Sham
Casp4	Caspase 4	Up-regulated
Cdkn1a	Cyclin dependent kinase inhibitor 1A	Up-regulated
Edem1	ER degradation enhancing alpha-mannosidase like protein 1	Up-regulated
Egfr	Epidermal growth factor receptor	Up-regulated
Hif1a	Hypoxia-inducible factors 1-alpha	Up-regulated
Myc	Myelocytomatosis	Up-regulated
Rgs19	Regulator of G protein signaling 19	Up-regulated

C

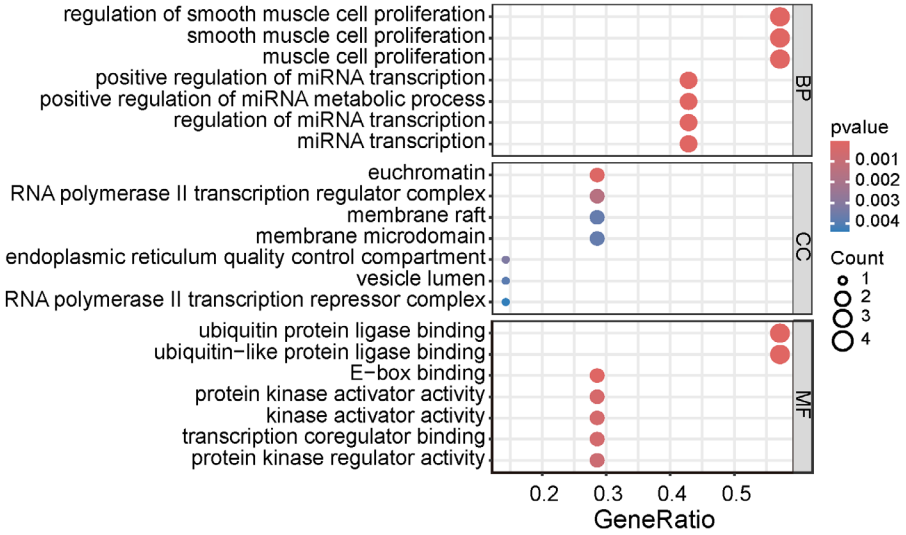

D

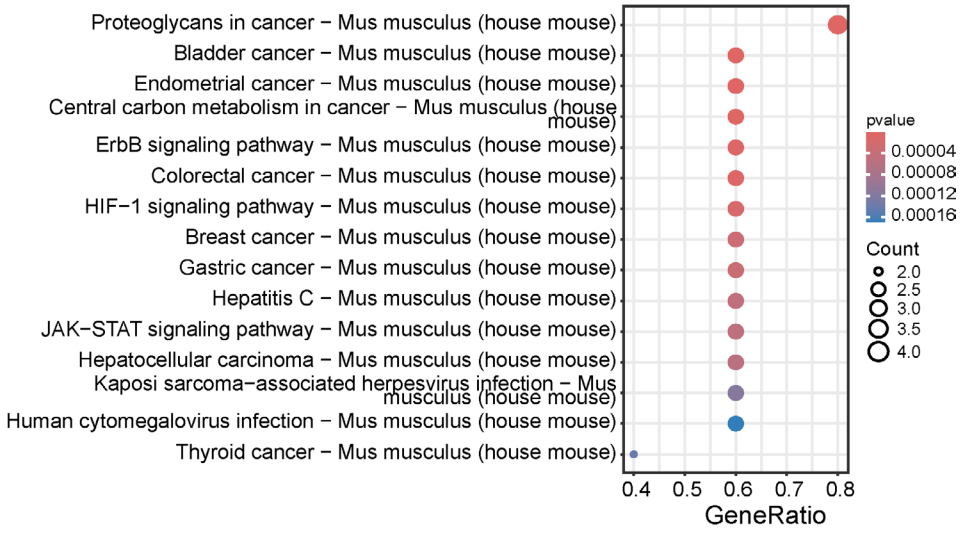

Fig. 2. Identification of autophagy-related differentially expressed genes (ARDEGs) and functional enrichment analysis. A. Venn diagram showing the shared genes between DEGs and autophagy-related genes; B. Table showing upregulation of all 7 shared genes in the I/R group; C,D. Gene Ontology (GO) and Kyoto Encyclopedia of Genes and Genomes (KEGG) enrichment analyses presented as bubble plots

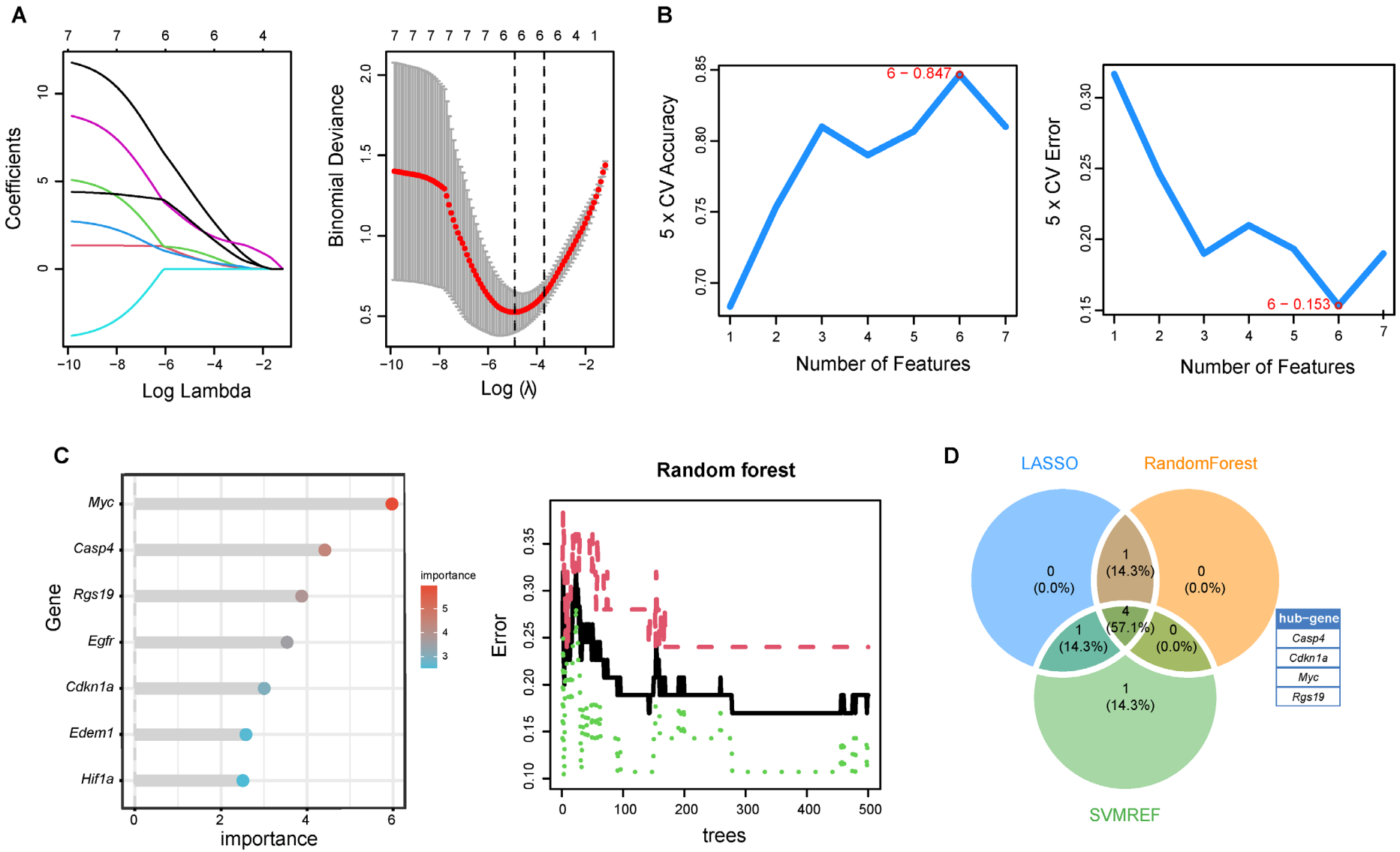

Fig. 3. Identification of candidate diagnostic biomarkers for myocardial ischemia/reperfusion (I/R) using 3 machine-learning algorithms. A. Six key genes identified using the least absolute shrinkage and selection operator (LASSO) model; B. Support vector machine–recursive feature elimination (SVM-RFE) identified 6 candidate genes associated with I/R; C. The top 7 candidate genes identifiedusing the Random Forest model; D. Venn diagram showing the 4 genes identified by all 3 machine-learning algorithms

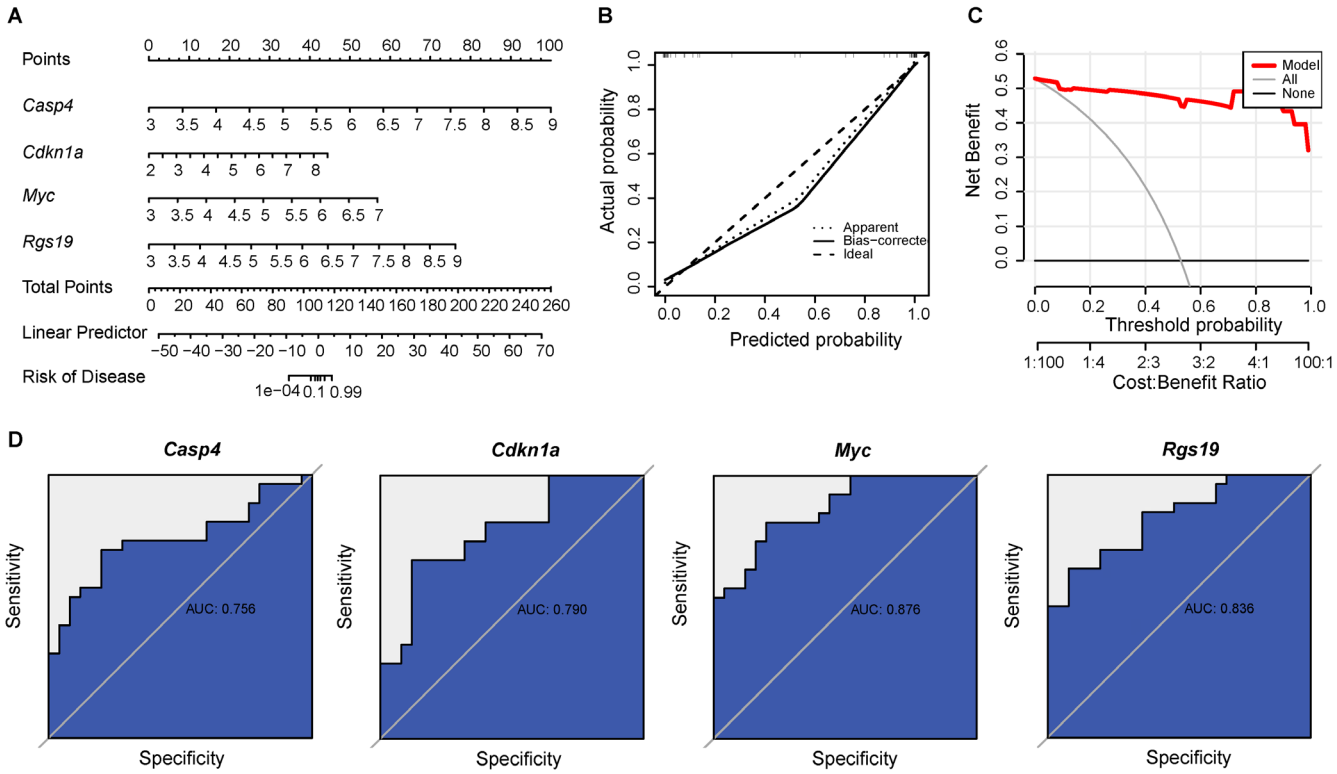

Fig. 4. Development of a nomogram for predicting myocardial ischemia/reperfusion (I/R) injury. A. Nomogram predicting the risk of myocardial I/R injury based on *Casp4*, *Cdkn1a*, *Myc*, and *Rgs19*; B. Calibration curve of the nomogram; C. Decision curve analysis of the nomogram; D. Receiver operating characteristic (ROC) curves of the 4 candidate biomarkers showing their diagnostic performance

tool (Fig. 4A). The calibration curve (Fig. 4B) demonstrated good agreement between the predicted and observed probabilities, indicating excellent calibration. In addition, decision curve analysis (Fig. 4C) demonstrated the potential clinical utility of the nomogram for the diagnosis of myocardial I/R injury. In the development cohort, the AUCs were 0.756 for Casp4, 0.790 for Cdkn1a, 0.876 for Myc, and 0.836 for Rgs19 (Fig. 4D), indicating high diagnostic accuracy and strong discriminatory performance.

Single-gene GSEA analysis of hub biomarkers

To investigate the potential biological functions associated with the diagnostic biomarkers, single-gene GSEA was performed, and the top 5 positively and negatively enriched pathways were visualized. The analysis demonstrated that the 4 hub genes were predominantly associated with metabolic pathways, including lipoic acid metabolism and propanoate metabolism. In addition, all 4 genes were enriched in pathways related to valine, leucine, and isoleucine degradation, as well as extracellular matrix (ECM)-receptor interaction (Fig. 5).

Association between immune cell infiltration and hub genes

Additionally, the CIBERSORT algorithm was used to estimate immune cell infiltration in the I/R and sham groups. As shown in Fig. 6A, significant differences in immune cell composition were observed between the 2 groups. Compared with the sham group, the I/R group exhibited increased infiltration of naïve $CD8^+$ T cells, M2 macrophages, and activated dendritic cells (DCs), whereas the sham group showed higher proportions of mast cells, plasma cells, memory $CD8^+$ T cells, and Th17 cells. Furthermore, correlation analysis suggested that the identified biomarker genes may contribute to the progression of I/R injury through interactions with multiple immune cell populations, including T cells, activated DCs, macrophages, neutrophils, and B cells (Fig. 6B–E).

Exploring subtypes of I/R with biological molecular mechanisms

To further characterize heterogeneity within the I/R group, unsupervised clustering analysis was performed to classify I/R samples into distinct molecular subtypes. Using the expression profiles of the 7 shared genes, consensus clustering was applied to 28 I/R samples. Two optimal subtypes were identified based on the consensus matrix, CDF plot, and relative changes in the area under the CDF curve (Fig. 7A). After

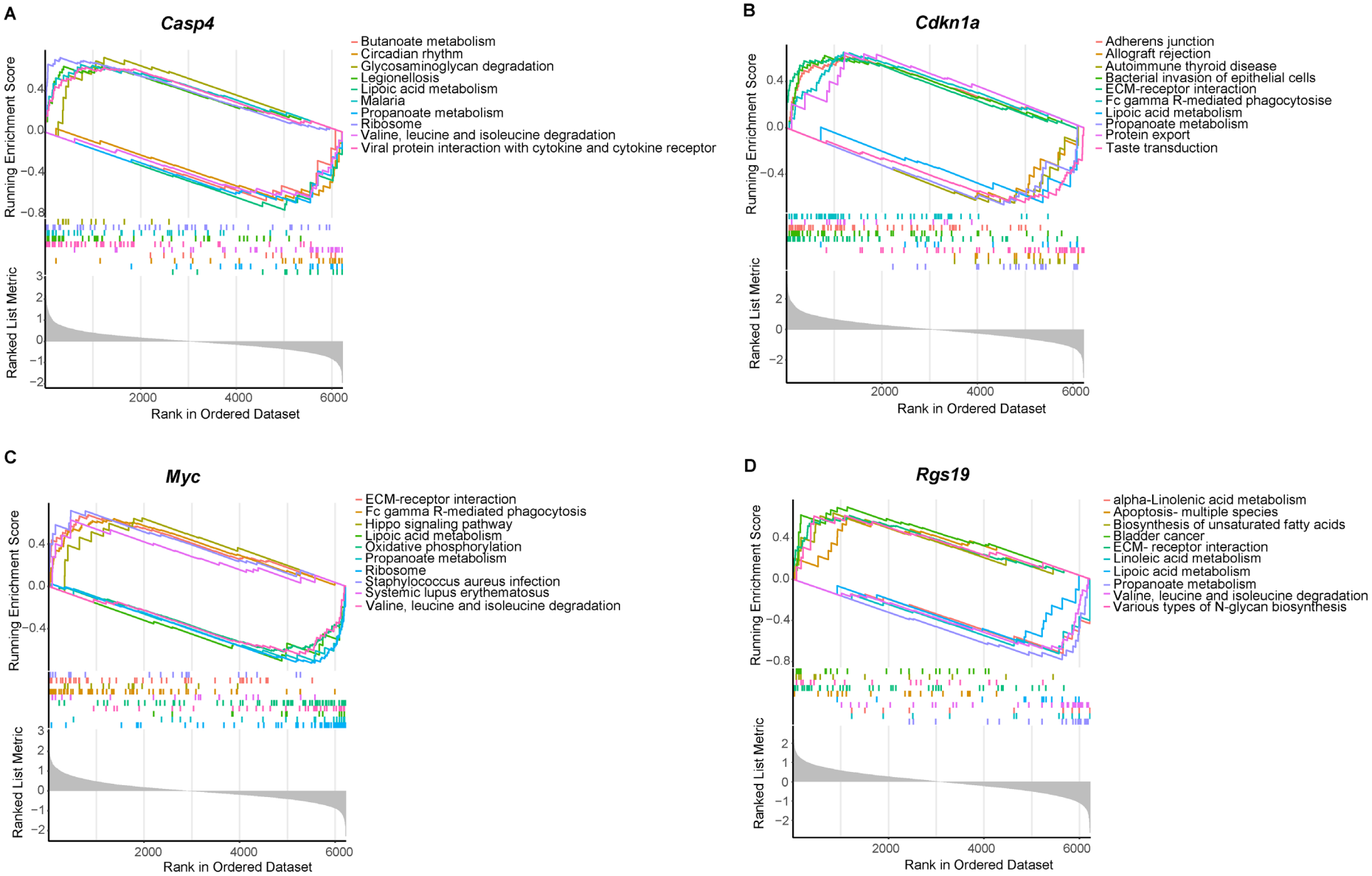

Fig. 5. Gene set enrichment analysis (GSEA) of the 4 signature genes. Enriched biological pathways associated with *Casp4* (A), *Cdkn1a* (B), *Myc* (C), and *Rgs19* (D) in myocardial ischemia/reperfusion (I/R)

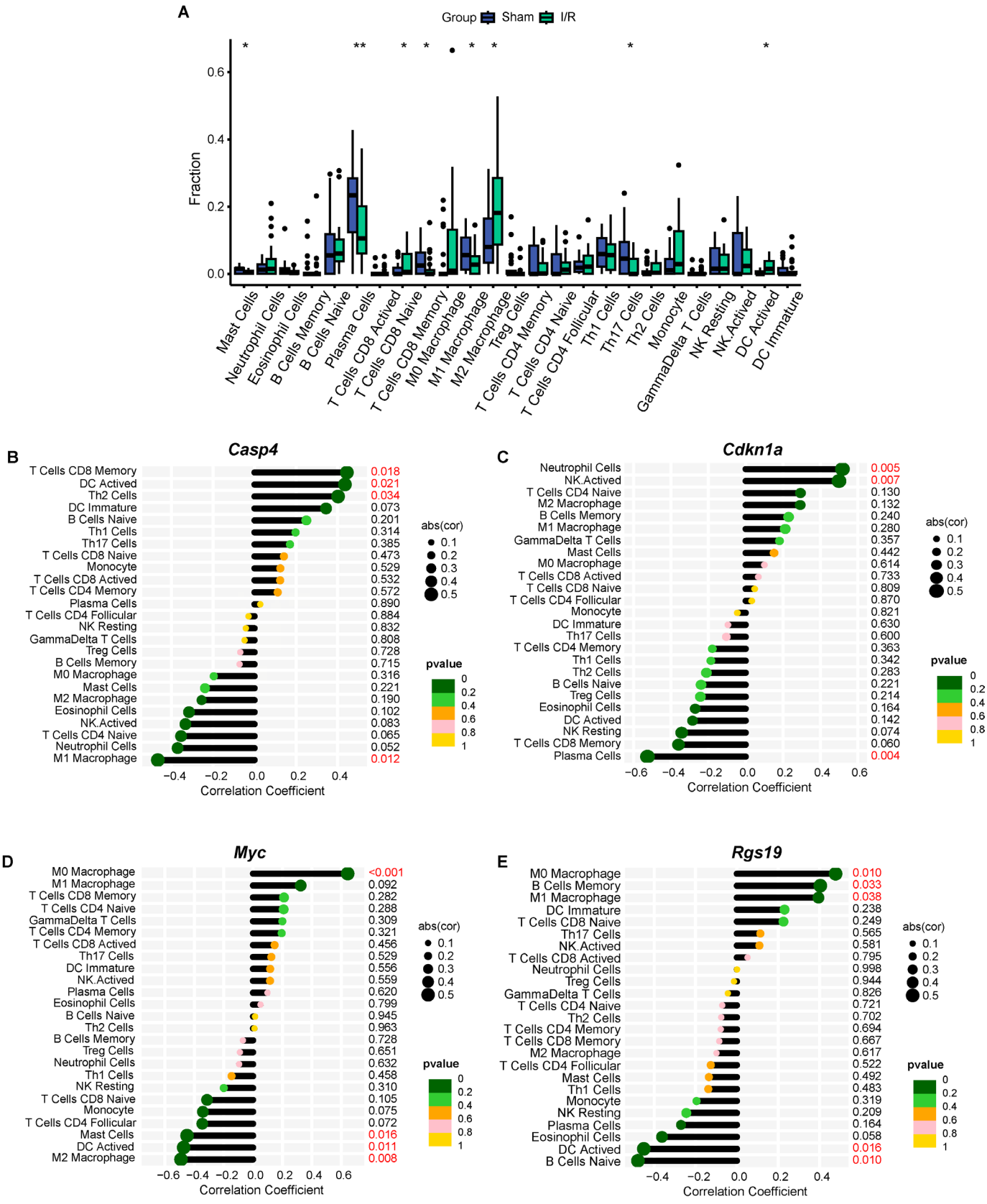

Fig. 6. Immune cell infiltration analysis. A. Distribution of 25 immune cell types between the sham and myocardial ischemia/reperfusion (I/R) groups; B–E. Correlations between immune cell abundance and the expression of the signature genes in I/R tissue (*p < 0.05, **p < 0.01)

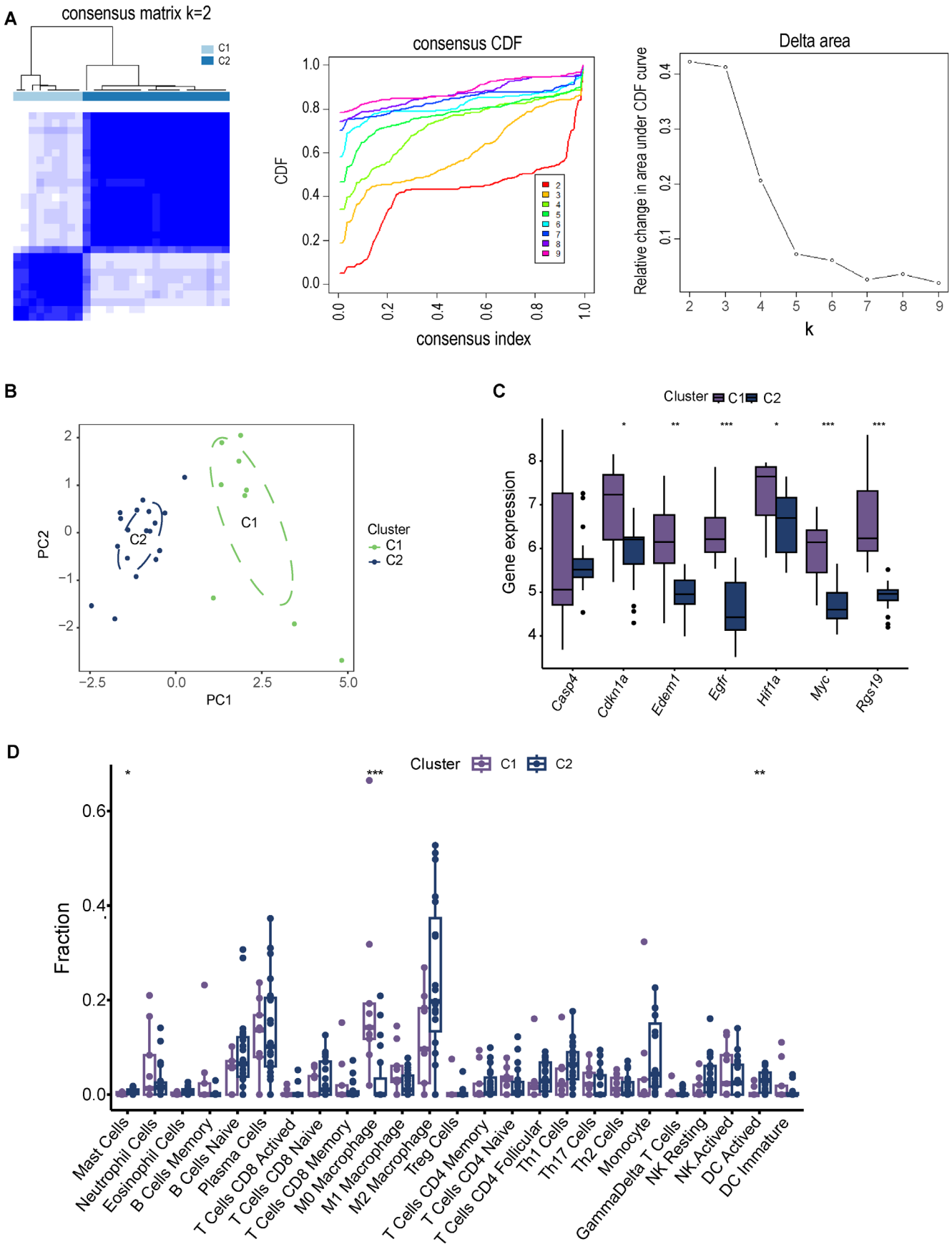

Fig. 7. Identification and characterization of distinct molecular subtypes in myocardial ischemia/reperfusion (I/R). A. Consensus clustering matrix, cumulative distribution function (CDF) curves, and CDF delta area plots identifying 2 clusters among the 28 I/R samples (k = 2); B. Principal component analysis (PCA) distinguishing the 2 subtypes based on the expression profiles of 7 autophagy-related differentially expressed genes (ARDEGs); C. Box plots showing the expression profiles of the 7 shared ARDEGs in the 2 subtypes; D. Distribution of immune cell infiltration across the 2 autophagy-related subtypes (*p < 0.05, **p < 0.01)

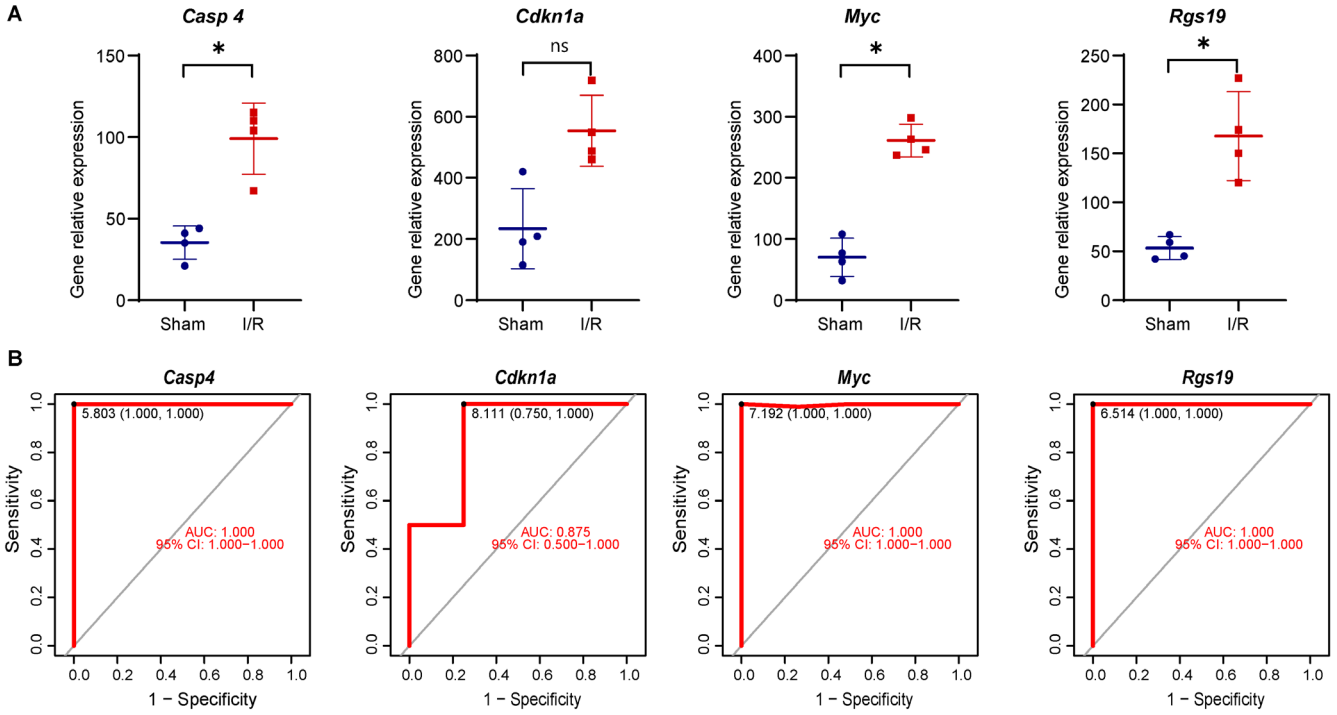

Fig. 8. Expression and diagnostic performance of the 4 hub genes in the GSE168610 dataset. A. Expression levels of *Casp4*, *Cdkn1a*, *Myc*, and *Rgs19* in the I/R group compared with the sham group. *Casp4*, *Myc*, and *Rgs19* were significantly increased ($p < 0.05$), whereas *Cdkn1a* was not significantly different ($p > 0.05$); B. Receiver operating characteristic (ROC) curves and areas under the curve (AUCs) for the 4 candidate biomarkers

classification into 2 subtypes (C1, n = 9; C2, n = 19), PCA demonstrated clear separation of the C1 and C2 groups based on gene expression profiles (Fig. 7B).

Further analysis of the shared genes revealed that, with the exception of *Casp4*, the C1 subtype exhibited significantly higher expression of *Cdkn1a*, *Edem1*, *Egfr*, *Hif1a*, *Myc*, and *Rgs19* than the C2 subtype (Fig. 7C). In addition, marked differences in immune cell abundance were observed between the 2 subtypes. The C2 subtype showed higher proportions of mast cells and activated DCs, whereas the C1 subtype exhibited greater infiltration of M0 macrophages (Fig. 7D).

To investigate functional differences between the 2 subtypes, KEGG and GO enrichment analyses were performed. As shown in Supplementary Fig. 3A,B, the DEGs between C1 and C2 were significantly enriched in pathways related to neurodegeneration, oxidative phosphorylation, Parkinson's disease, and cardiac muscle contraction. Gene Ontology enrichment analysis further demonstrated significant enrichment of biological processes related to cellular respiration, energy metabolism, mitochondrial protein complexes, structural constituents of the ribosome, and proton transmembrane transporter activity.

Hub genes expression and diagnostics in GSE168610

To validate the reliability of the bioinformatics analysis, the 4 key genes were independently evaluated in the external validation cohort (GSE168610). As shown in Fig. 8A, the expression levels of *Casp4*, *Myc*, and *Rgs19* were significantly increased in I/R myocardial tissue compared with sham controls ($p < 0.05$), whereas *Cdkn1a* expression did not differ significantly (ns, $p > 0.05$). Furthermore, ROC curve analysis (Fig. 8B) demonstrated that *Casp4*, *Myc*, and *Rgs19* showed perfect diagnostic performance for distinguishing I/R injury (AUC = 1.000), whereas *Cdkn1a* also demonstrated excellent diagnostic performance (AUC = 0.875).

Preliminary validation of autophagy-related prognostic genes in myocardial I/R and CMECs H/R model

To validate the roles of *Casp4*, *Cdkn1a*, *Myc*, and *Rgs19* identified through bioinformatics analysis, an in vivo myocardial I/R-induced microvascular injury model and an in vitro H/R model were established to evaluate the expression of these candidate biomarkers. Electrocardiographic analysis revealed significant ST-segment elevation during myocardial ischemia, which decreased by more than 50% after reperfusion (Supplementary Fig. 1A). TTC/Evans blue staining demonstrated a marked increase in infarct size following I/R injury (Supplementary Fig. 1B and Supplementary Table 6). After I/R, cardiac function was significantly impaired, as evidenced by reduced LVEF and LVFS (Supplementary Fig. 1C,D and Supplementary Table 6). Gelatin–ink staining further confirmed impaired microvascular perfusion in myocardial tissue after I/R (Supplementary Fig. 1E and Supplementary Table 6). Myocardial tissue subjected to I/R exhibited significantly increased mRNA expression

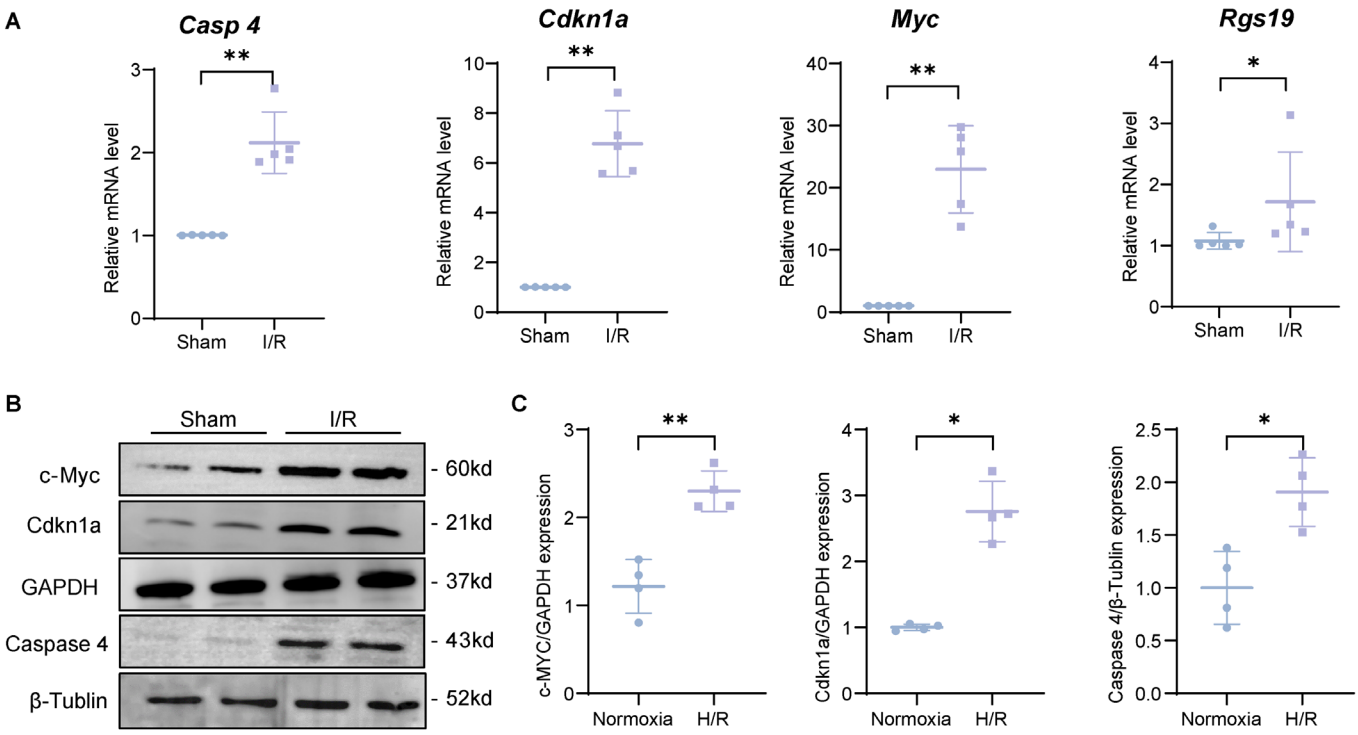

Fig. 9. Expression of 4 hub-gene mRNAs and 3 corresponding proteins in myocardial I/R injury. A. mRNA expression levels of *Myc*, *Casp4*, *Cdkn1a*, and *Rgs19* (Mann–Whitney U test; n = 5); B,C. Western blot analysis and quantification of c-Myc, Caspase-4, and p21 (Mann–Whitney U test; n = 4). RGS19 protein was not assessed (*p < 0.05,**p < 0.01)

Table 1. The mRNA expression levels of *Casp4*, *Cdkn1a*, *Myc*, and *Rgs19* were compared between the sham and myocardial ischemia/reperfusion (I/R) groups and between the normoxia and hypoxia/reoxygenation (H/R) groups using Welch's t test or the Mann–Whitney U test (Fig. 9A and Supplementary Fig. 5A)

Genes	Groups	Samples (n)	Median (Q1, Q3)	U statistic	p-value
Casp4	sham	5	1.00 (1.00, 1.01)	U = 0	0.008**
	I/R	5	1.98 (1.90, 2.41)		
	normoxia	6	1.00 (1.00, 1.01)	U = 0	0.002**
	H/R	6	2.24 (2.14, 2.31)		
Cdkn1a	sham	5	1.01 (1.00, 1.01)	U = 0	0.008**
	I/R	5	5.56 (5.51, 5.68)		
	normoxia	6	1.00 (1.00, 1.01)	U = 0	0.002**
	H/R	6	2.27 (1.38, 3.18)		
Myc	sham	5	1.02 (1.01, 1.17)	U = 0	0.008**
	I/R	5	25.88 (16.49, 28.92)		
	normoxia	6	1.01 (1.001, 1.02)	U = 0	0.002**
	H/R	6	1.58 (1.32, 2.15)		
Rgs19	sham	5	1.02 (1.01, 1.04)	U = 2	0.032*
	I/R	5	1.35 (1.23, 1.23)		
	normoxia	6	1.01 (1.00, 1.03)	U = 0	0.002**
	H/R	6	2.72 (1.78, 3.80)		

*p < 0.05, **p < 0.01.

of *Casp4*, *Cdkn1a*, *Myc*, and *Rgs19* compared with sham controls (Fig. 9A and Table 1), together with increased protein expression of caspase-4, p21, and c-Myc (U = 0, p < 0.05; Fig. 9B and Table 2). Immunohistochemistry confirmed enrichment of caspase-4 and c-Myc within areas of microvascular injury (Supplementary Fig. 4A,B).

In addition, RT-qPCR demonstrated H/R-induced up-regulation of *Casp4*, *Cdkn1a*, *Myc*, and *Rgs19* compared with normoxic controls, whereas increased protein expression of caspase-4, p21, and c-Myc was confirmed with western blot (WB) analysis (Supplementary Fig. 5A–C and Tables 1,2).

Table 2. Protein expression levels of caspase-4, Cdkn1a, and c-Myc were compared between the sham and myocardial ischemia/reperfusion (I/R) groups and between the normoxia and hypoxia/reoxygenation (H/R) groups using the Mann–Whitney U test (Fig. 9B,C and Supplementary Fig. 5B,C)

Genes	Group	Samples, n	Median (Q1, Q3)	U statistic	p-value
Caspase-4	sham	4	1.00 (0.90, 1.10)	U = 0	0.029*
	I/R	4	2.54 (2.29, 2.70)		
	normoxia	4	1.00 (0.77, 1.23)	U = 0	0.029*
	H/R	4	1.90 (1.69, 2.11)		
p21	sham	4	1.00 (0.94, 1.11)	U = 0	0.029*
	I/R	4	2.70 (2.59, 3.50)		
	normoxia	4	1.00 (0.96, 1.04)	U = 0	0.029*
	H/R	4	2.70 (2.47, 3.05)		
c-Myc	sham	4	1.12 (0.98, 1.17)	U = 0	0.029*
	I/R	4	2.45 (2.39, 2.58)		
	normoxia	4	1.27 (1.05, 1.43)	U = 0	0.029*
	H/R	4	2.22 (2.13, 2.47)		

*p < 0.05, **p < 0.01.

Myc knockout reduces apoptosis in H/R-induced CMECs

We performed TUNEL staining to detect apoptosis. As shown in Fig. 10A,B and Table 3, the apoptotic rate of vascular endothelial cells was significantly higher in the H/R group than in the normoxia group. This increase was almost completely reversed by si-Myc treatment. Western blot analysis demonstrated that H/R injury significantly upregulated Bax expression, downregulated Bcl-2 expression, and promoted LC3-II conversion, whereas Myc knockout largely normalized these alterations in protein expression ($p < 0.05$; Fig. 10C,D and Table 4). Transmission electron microscopy was then used to examine mitochondrial ultrastructure and autophagosome formation. In cells exposed to H/R injury, mitochondria exhibited marked swelling and disruption of the cristae, accompanied by abundant autophagic vacuoles. In contrast, si-Myc treatment markedly ameliorated these ultrastructural alterations (Supplementary Fig. 6).

Discussion

Despite clinical efforts to restore blood flow to the ischemic myocardium and limit myocardial necrosis, myocardial I/R continues to damage both cardiac tissue and the coronary microcirculation.[21] Extensive microvascular injury impairs myocardial perfusion and limits the delivery of therapeutic agents to the distal microvasculature, thereby complicating clinical management.[22] By integrating machine-learning approaches with multimodal validation, we identified a potential 4-biomarker panel (*Casp4*, *Cdkn1a*, *Myc*, and *Rgs19*) with high diagnostic accuracy (AUCs of 0.756 for Casp4, 0.790 for Cdkn1a, 0.876 for Myc, and 0.836 for Rgs19; Fig. 4D) for microvascular I/R injury. Importantly, c-Myc emerged as a dual-function regulator: beyond its diagnostic value, c-Myc knockout significantly reduced endothelial apoptosis and autophagic dysregulation (Fig. 10A–D), highlighting its potential as a therapeutic target. This finding directly addresses a persistent challenge in reperfusion therapy. Although rapid revascularization remains essential for the treatment of ischemic cardiomyopathy, it paradoxically induces microvascular I/R injury that compromises treatment efficacy. The dual protective and detrimental roles of autophagy in cardiac I/R make this pathway an attractive therapeutic target. Our data indicate that dysregulated autophagy, particularly excessive c-Myc-mediated autophagy, is a key mechanism underlying this paradox. This mechanistic insight identifies a potential therapeutic target for mitigating the no-reflow phenomenon, which limits drug delivery and tissue perfusion.

Casp4 has been reported to mediate pyroptosis in microvascular endothelial cells and to play a critical role in the pathophysiology of myocardial I/R.[18] Our findings are consistent with previous studies, demonstrating a significant upregulation of *Casp4* expression in both the I/R and H/R models. Previous research has also suggested that inhibition of *Casp4*-mediated cell death through activation of autophagy signaling pathways may represent a promising therapeutic strategy for myocardial reperfusion-related microvascular injury.[18] Given its prognostic significance and overexpression in clear cell renal cell carcinoma, *Casp4* has also emerged as a candidate biomarker for disease monitoring and a potential molecular target for therapeutic intervention.[23] During cardiac I/R, cells are exposed to hypoxia, nutrient deprivation, inflammation, and oxidative stress, resulting in dysregulated cell-cycle progression and subsequent cellular dysfunction and injury. *Cdkn1a* (*p21*), a cyclin-dependent kinase inhibitor, plays a protective role in I/R injury by limiting cell-cycle progression and reducing oxidative stress.[24] Previous studies have shown that *Cdkn1a* interacts with the autophagy-related protein LC3B, thereby contributing to the attenuation of cardiac

Table 3. Differences in TUNEL-positive cell quantification among the experimental groups were analyzed using one-way analysis of variance (ANOVA) followed by Tukey's post hoc test (Fig. 10A,B)

Variable	Group comparison	Mean ±SD	ANOVA F-value	df	ANOVA p-value	Tukey's q-value	Tukey's p-value
TUNEL staining	normoxia vs H/R	0.21 ±0.05 vs 32.50 ±6.32	1.67	(3, 8)	0.449	6.59	0.007**
	H/R + siNC vs H/R + si-Myc	35.20 ±4.65 vs 10.58 ±2.02				5.05	0.030*

df – degrees of freedom; Tukey's q – Tukey's honestly significant difference (HSD) test statistic; I/R – ischemia/reperfusion; H/R – hypoxia/reoxygenation; SD – standard deviation; siNC – small interfering RNA negative control; si-Myc – small interfering RNA targeting Myc; *p < 0.05, **p < 0.01.

Table 4. Protein expression levels of c-Myc, Bax, Bcl-2, and LC3-II/I were compared using one-way analysis of variance (ANOVA) followed by Tukey's post hoc test for the following comparisons: normoxia vs H/R and H/R + siNC vs H/R + si-Myc (Fig. 10C,D)

Genes	Group comparison	Mean ±SD	ANOVA F-value	df	ANOVA p-value	Tukey's q-value	Tukey's p-value
c-Myc	normoxia vs H/R	0.38 ±0.01 vs 1.03 ±0.25	1.67	(3, 8)	0.449	6.59	0.007**
	H/R + siNC vs H/R + si-Myc	0.92 ±0.19 vs 0.42 ±0.04				5.05	0.030*
Bax	normoxia vs H/R	0.45 ±0.12 vs 1.04 ±0.04	0.980	(3, 8)	0.208	5.74	0.015*
	H/R + siNC vs H/R + si-Myc	1.03 ±0.07 vs 0.37 ±0.03				6.08	0.011*
Bcl2	normoxia vs H/R	0.95 ±0.21 vs 0.48 ±0.20	1.90	(3, 8)	0.376	13.66	<0.001**
	H/R + siNC vs H/R + si-Myc	0.49 ±0.21 vs 0.85 ±0.33				9.29	<0.001**
LC3II/I	normoxia vs H/R	1.15 ±0.46 vs 3.12 ±0.73	2.25	(3, 8)	0.160	7.15	0.004**
	H/R + siNC vs H/R + si-Myc	2.97 ±0.40 vs 1.46 ±0.28				5.42	0.021*

df – degrees of freedom; Tukey's q – Tukey's honestly significant difference (HSD) test statistic; I/R – ischemia/reperfusion; H/R – hypoxia/reoxygenation; SD – standard deviation; siNC – small interfering RNA negative control; si-Myc – small interfering RNA targeting Myc; *p < 0.05, **p < 0.01.

dysfunction.[25] Moreover, activation of *Cdkn1a*-mediated cell-cycle arrest has been shown to alleviate injury in cardiac microvascular endothelial cells.[26] Multiomics data derived from human cardiac cells have also identified *Cdkn1a* as a potential therapeutic target for heart failure.[27] Our study demonstrated a marked increase in *Cdkn1a* expression in myocardial I/R tissue and, to our knowledge, is the first to document significant upregulation of *Cdkn1a* in H/R-treated CMECs. These findings underscore the pivotal role of *Cdkn1a* in the progression of myocardial I/R-induced microvascular injury and highlight its potential as a therapeutic target for this condition.

The *Myc* oncogene encodes a potent transcription factor that regulates nearly every cellular process through interactions with numerous transcriptional regulators and protein complexes.[28] The *Myc* family comprises 3 members: *Myc* (*c-Myc*), *Mycl*, and *Mycn*, with c-Myc being particularly relevant to cardiomyocytes. Previous studies have indicated that c-Myc overexpression may contribute to cardiomyocyte apoptosis following myocardial I/R.[29] Research has also suggested that regulation of *Myc* expression and its downstream signaling pathways is essential for maintaining cellular integrity and function under cardiac stress.[30] Evidence further indicates that selective inhibition of *c-Myc* overexpression in cardiomyocytes may represent a novel therapeutic strategy for cardiac hypertrophy.[31] In our study, *c-Myc* knockout alleviated H/R-induced microvascular injury, suggesting that *c-Myc* may represent a promising therapeutic target for myocardial I/R injury. Aberrant *Myc* expression in cardiac tissue has also been proposed as a potential biomarker for predicting outcomes in patients with septic cardiomyopathy.[32]

The clinical relevance of *Myc* expression is further supported by human transcriptomic datasets. Analysis of GSE59867 (peripheral blood samples from 312 patients after myocardial infarction) demonstrated >2-fold upregulation of *Myc* compared with controls ($p < 0.001$), whereas GSE60993 (human ischemic myocardium) showed a significant correlation between *Myc* expression and infarct severity ($r = 0.68$, $p < 0.01$).[33,34] These findings support the potential role of *Myc* as both a diagnostic biomarker and a therapeutic target in ischemic injury. However, previous studies have also shown that *Myc* downregulation may exacerbate cardiomyocyte apoptosis and oxidative stress, thereby aggravating myocardial I/R injury.[35] This apparent discrepancy may reflect differences in animal

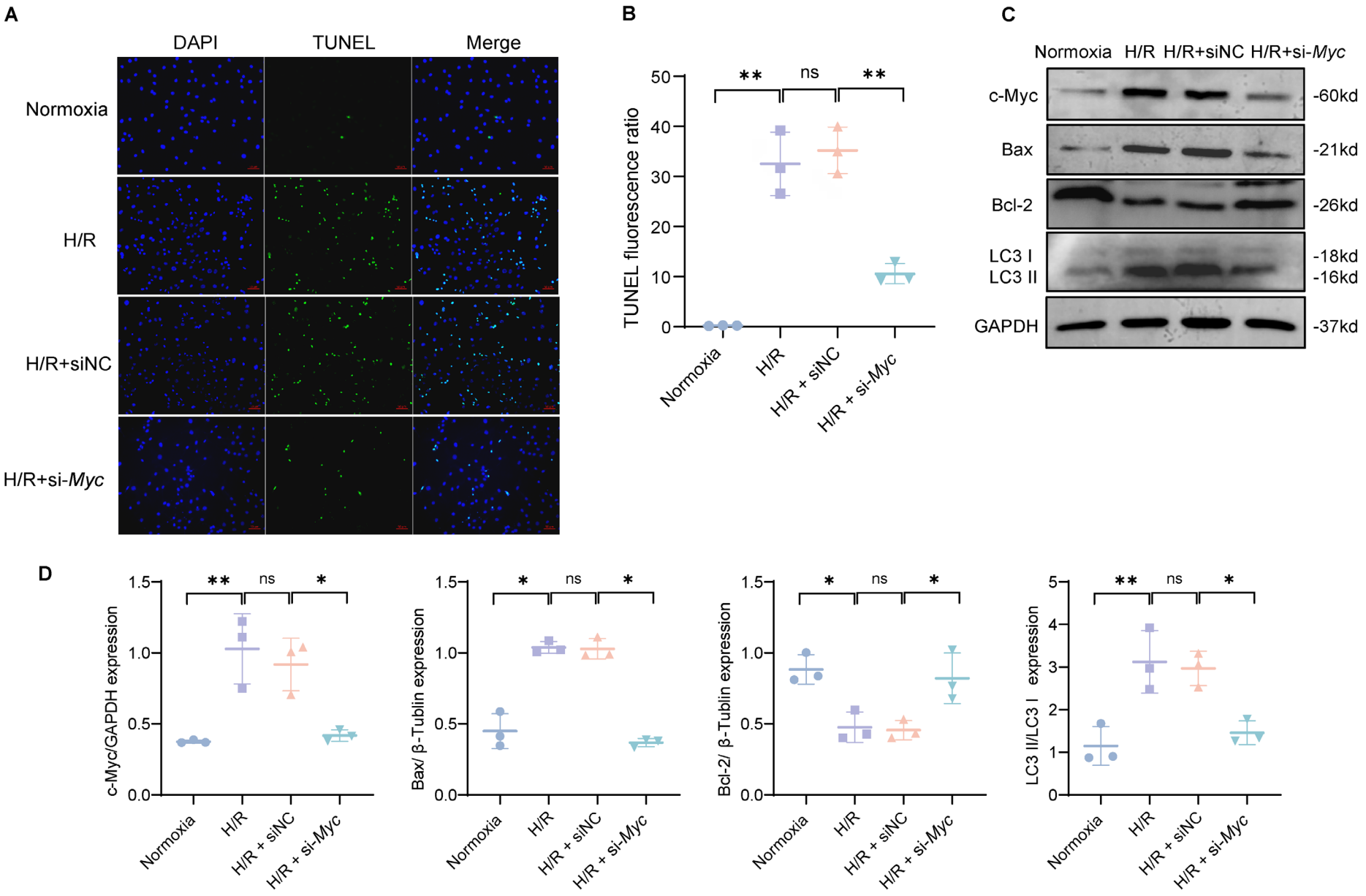

Fig. 10. *Myc* knockout attenuates hypoxia/reoxygenation (H/R)-induced apoptosis and excessive autophagy. A. TUNEL/DAPI immunofluorescence staining showing apoptotic cells (green) in normoxic, H/R-treated, and *Myc* knockdown H/R cells (n = 3). Scale bar: 20 μm; B. Quantification of TUNEL-positive cells (n = 3); C. Western blot (WB) analysis of c-Myc, Bax, Bcl-2, LC3-I, and LC3-II (n = 3); D. Quantification of the relative protein expression levels of c-Myc, Bax, Bcl-2, LC3-I, and LC3-II. Data are presented as the mean ± standard deviation (SD) (*p < 0.05, **p < 0.01); one-way analysis of variance (ANOVA) with Tukey's post hoc test)

and cellular models, as well as variations in the duration and experimental protocols of I/R.

Rgs19, a member of the regulator of G protein signaling (RGS) family, modulates G protein-coupled receptor (GPCR) signaling by accelerating GTP hydrolysis of Gα subunits, thereby acting as a negative regulator of intracellular signaling. According to previous studies, *Rgs19* influences cardiomyocyte differentiation and cardiac development through the Wnt/β-catenin signaling pathway. Transgenic mice overexpressing *Rgs19* exhibit increased expression of heart failure markers, enhanced cell proliferation, and abnormal ventricular repolarization.[36] Overexpression of *Rgs19* has also been reported in several cancers and is associated with poor clinical outcomes.[37,38] However, little is known about the role of *Rgs19* in myocardial I/R-induced microvascular dysfunction. Our study is the first to demonstrate significant upregulation of *Rgs19* in myocardial I/R-induced microvascular injury, suggesting that it may play an important role in the pathogenesis of this condition.

Furthermore, we developed a nomogram incorporating the 4 biomarker genes. This integrated model demonstrated a high AUC together with excellent calibration, indicating good diagnostic performance and reliability for detecting myocardial I/R injury. Implementation of this tool in clinical practice may improve the early identification of microvascular complications associated with myocardial I/R.

Further GSEA suggested that the pathogenesis of myocardial I/R may be associated with disturbances in citric acid cycle metabolism involving the 4 diagnostic genes. Substantial evidence indicates that myocardial I/R is closely associated with abnormalities in glucose and lipid metabolism.[39] These findings suggest that the 4 hub genes may participate in metabolic regulation during myocardial I/R and provide new insights into potential therapeutic targets. Myocardial I/R is also closely associated with immune regulation. During myocardial I/R injury, infiltration of immune cells, including macrophages and T lymphocytes, contributes to the inflammatory response.[40] In the early phase of reperfusion, activated neutrophils markedly increase reactive oxygen species (ROS) production, thereby exacerbating cardiomyocyte necrosis.[41] Significant differences in immune cell abundance were observed between the 2 groups, and the expression of the biomarker genes was closely associated with the infiltration of multiple immune cell populations, including T cells, B cells, activated DCs, natural killer (NK) cells, and, in particular, macrophages. Macrophages, which play a pivotal role in the immune response to myocardial I/R, are commonly classified into M0, M1, and M2 subtypes. M2 macrophages exhibit anti-inflammatory and tissue-protective properties, whereas M1 macrophages promote inflammation and tissue injury.[42] These findings suggest that the 4 hub genes may play important roles in immune regulation during myocardial I/R injury.

Moreover, an unsupervised clustering approach identified 2 molecular subtypes based on the expression profiles of 7 autophagy-related regulators. Functional enrichment analysis revealed that the C2 subtype was associated with oxidative phosphorylation, ROS generation, and the mitochondrial respiratory chain complex, all of which are involved in the regulation of autophagy.[43,44] These findings suggest that the C2 subtype may be closely associated with autophagy dysregulation, which could have important implications for the early detection and treatment of myocardial I/R injury. Given the poor prognosis associated with the no-reflow phenomenon resulting from myocardial microvascular injury, the upregulation of the 4 autophagy-related hub genes identified in this study may represent potential therapeutic targets. These findings provide new insights into the molecular mechanisms of autophagy in myocardial I/R and may contribute to the development of improved strategies for the early diagnosis and treatment of this condition, ultimately improving patient outcomes.

Limitations of the study

However, this study has several limitations. First, evaluation of the therapeutic efficacy of c-Myc inhibition in animal models that more closely mimic human cardiac pathophysiology is needed. Second, the data analyzed in this study were obtained from the GEO database, and suitable human datasets were not available. Furthermore, the expression profiles of the 4 key genes were validated only in animal models and cell-based experiments and therefore require further validation in human cohorts. Future validation should include prospective studies evaluating serum biomarkers using enzyme-linked immunosorbent assay (ELISA) or Luminex assays in relation to cardiac magnetic resonance imaging (cMRI)-quantified microvascular obstruction (MVO) and the no-reflow phenomenon after percutaneous coronary intervention (PCI) in patients with ST-segment elevation myocardial infarction (STEMI). Such studies would establish the clinical utility of these biomarkers for predicting the no-reflow phenomenon and guiding adjuvant therapies. In addition, further investigation of the molecular mechanisms and signaling pathways involving these genes in myocardial I/R-induced microvascular injury is warranted.

Conclusions

This study is the first to identify autophagy-related biomarkers (*Myc*, *Casp4*, *Cdkn1a*, and *Rgs19*) associated with microvascular injury in cardiac I/R using integrated machine learning and experimental validation. We identified *c-Myc* as a pivotal regulator linking autophagic dysregulation to endothelial injury, with *c-Myc* knockout demonstrating significant therapeutic potential. These findings highlight *c-Myc* inhibition as a novel treat-to-target

therapeutic strategy for reperfusion injury, warranting clinical validation in STEMI cohorts and the development of point-of-care diagnostics. Our findings may also inform the future development of biomarker-guided strategies for the early detection and therapeutic modulation of cardiac microvascular I/R injury.

Supplementary data

The Supplementary materials are available at https://doi.org/10.5281/zenodo.22122481. The package includes the following files:

Supplementary Fig. 1. Cardiac I/R establishment and microvascular injury evaluation.

Supplementary Fig. 2. Bioinformatic analysis of GSE168610: PCA, differential expression, and autophagy gene overlap in I/R model.

Supplementary Fig. 3. GO and KEGG pathway analysis for distinct I/R subgroup.

Supplementary Fig. 4. Immunohistochemical (IHC) staining of *c-Myc* and *Caspase 4* in myocardial I/R.

Supplementary Fig. 5. Changes in mRNA and protein expression levels of the hub biomarkers in the H/R mode.

Supplementary Fig. 6. Observation of cellular autophagosome.

Supplementary Table 1. Specific information of datasets.

Supplementary Table 2. The primer sequences used for RT-qPCR.

Supplementary Table 3. Validation of key gene expression in the dataset GSE168610.

Supplementary Table 4. Power analysis of endpoint assays in myocardial I/R model.

Supplementary Table 5. Assessment of parametric test assumptions and selection of statistical methods for genes expression and TUNEL fluorescence intensity analysis.

Supplementary Table 6. Mann–Whitney U tests performed to compare 4 cardiac and functional parameters between sham and I/R groups (Supplementary Fig. 1B–E).

Data Availability Statement

The datasets supporting the findings of the current study are openly available in Zenodo at https://doi.org/10.5281/zenodo.17137494.

AI and AI-assisted technologies usage

Not applicable.

ORCID iDs

Lina Tan https://orcid.org/0009-0005-2079-9432
Jingjing Rao https://orcid.org/0009-0003-6019-4388
Yue Wang https://orcid.org/0009-0004-6010-4423
Liangbo Hu https://orcid.org/0009-0001-3969-6477
Min He https://orcid.org/0009-0006-2357-6266
Jinyuan Tan https://orcid.org/0009-0009-1595-1590
Xiaocong Zeng https://orcid.org/0000-0002-6430-7736

References

1. Khan MA, Hashim MJ, Mustafa H, et al. Global epidemiology of ischemic heart disease: Results from the Global Burden of Disease Study. *Cureus*. 2020;12(7):e9349. doi:10.7759/cureus.9349
2. Yu G, Gong X, Xu Y, et al. The global burden and trends of four major types of heart disease, 1990–2019: A systematic analysis for the Global Burden of Disease Study 2019. *Public Health*. 2023;220:1–9. doi:10.1016/j.puhe.2023.04.005
3. Zhang S, Yan F, Luan F, et al. The pathological mechanisms and potential therapeutic drugs for myocardial ischemia reperfusion injury. *Phytomedicine*. 2024;129:155649. doi:10.1016/j.phymed.2024.155649
4. Sagris M, Apostolos A, Theofilis P, et al. Myocardial ischemia–reperfusion injury: Unraveling pathophysiology, clinical manifestations, and emerging prevention strategies. *Biomedicines*. 2024;12(4):802. doi:10.3390/biomedicines12040802
5. Reffelmann T, Kloner RA. The no-reflow phenomenon: A basic mechanism of myocardial ischemia and reperfusion. *Basic Res Cardiol*. 2006;101(5):359–372. doi:10.1007/s00395-006-0615-2
6. Gupta S, Gupta MM. No reflow phenomenon in percutaneous coronary interventions in ST-segment elevation myocardial infarction. *Indian Heart J*. 2016;68(4):539–551. doi:10.1016/j.ihj.2016.04.006
7. Scarabelli T, Stephanou A, Rayment N, et al. Apoptosis of endothelial cells precedes myocyte cell apoptosis in ischemia/reperfusion injury. *Circulation*. 2001;104(3):253–256. doi:10.1161/01.CIR.104.3.253
8. Li C, Ma Q, Toan S, Wang J, Zhou H, Liang J. SERCA overexpression reduces reperfusion-mediated cardiac microvascular damage through inhibition of the calcium/MCU/mPTP/necroptosis signaling pathways. *Redox Biol*. 2020;36:101659. doi:10.1016/j.redox.2020.101659
9. Battson ML, Lee DM, Gentile CL. Endoplasmic reticulum stress and the development of endothelial dysfunction. *Am J Physiol Heart Circ Physiol*. 2017;312(3):H355–H367. doi:10.1152/ajpheart.00437.2016
10. Zhong J, Ouyang H, Sun M, et al. Tanshinone IIA attenuates cardiac microvascular ischemia–reperfusion injury via regulating the SIRT1-PGC1α-mitochondrial apoptosis pathway. *Cell Stress Chaperones*. 2019;24(5):991–1003. doi:10.1007/s12192-019-01027-6
11. Wang J, Toan S, Zhou H. New insights into the role of mitochondria in cardiac microvascular ischemia/reperfusion injury. *Angiogenesis*. 2020;23(3):299–314. doi:10.1007/s10456-020-09720-2
12. Lavandero S, Chiong M, Rothermel BA, Hill JA. Autophagy in cardiovascular biology. *J Clin Invest*. 2015;125(1):55–64. doi:10.1172/JCI73943
13. Hu F, Hu T, Qiao Y, et al. Berberine inhibits excessive autophagy and protects myocardium against ischemia/reperfusion injury via the RhoE/AMPK pathway. *Int J Mol Med*. 2024;53(5):49. doi:10.3892/ijmm.2024.5373
14. Takagaki Y, Lee SM, Dongqing Z, Kitada M, Kanasaki K, Koya D. Endothelial autophagy deficiency induces IL6-dependent endothelial mesenchymal transition and organ fibrosis. *Autophagy*. 2020;16(10):1905–1914. doi:10.1080/15548627.2020.1713641
15. Chen WR, Liu HB, Chen YD, et al. Melatonin attenuates myocardial ischemia/reperfusion injury by inhibiting autophagy via an AMPK/mTOR signaling pathway. *Cell Physiol Biochem*. 2018;47(5):2067–2076. doi:10.1159/000491474
16. Li J, Wang Y, Wang C, et al. Shenlian extract decreases mitochondrial autophagy to regulate mitochondrial function in microvascular to alleviate coronary artery no-reflow. *Phytother Res*. 2023;37(5):1864–1882. doi:10.1002/ptr.7703
17. Cai C, Guo Z, Chang X, et al. Empagliflozin attenuates cardiac microvascular ischemia/reperfusion through activating the AMPKα1/ULK1/FUNDC1/mitophagy pathway. *Redox Biol*. 2022;52:102288. doi:10.1016/j.redox.2022.102288
18. Sun W, Lu H, Dong S, et al. Beclin1 controls caspase-4 inflammsome activation and pyroptosis in mouse myocardial reperfusion-induced microvascular injury. *Cell Commun Signal*. 2021;19(1):107. doi:10.1186/s12964-021-00786-z
19. Lin J, Lai X, Fan X, et al. Oridonin protects against myocardial ischemia–reperfusion injury by inhibiting GSDMD-mediated pyroptosis. *Genes (Basel)*. 2022;13(11):2133. doi:10.3390/genes13112133
20. Kujawa K, Bombała W, Kopszak A, et al. New statistical guidelines for manuscripts submitted to *Advances in Clinical and Experimental Medicine*. *Adv Clin Exp Med*. 2025;34(7):1085–1090. doi:10.17219/acem/206009

21. Zhao BH, Ruze A, Zhao L, et al. The role and mechanisms of microvascular damage in the ischemic myocardium. *Cell Mol Life Sci*. 2023; 80(11):341. doi:10.1007/s00018-023-04998-z
22. Heusch G. Coronary microvascular obstruction: The new frontier in cardioprotection. *Basic Res Cardiol*. 2019;114(6):45. doi:10.1007/s00395-019-0756-8
23. Meng L, Tian Z, Long X, et al. Caspase 4 overexpression as a prognostic marker in clear cell renal cell carcinoma: A study based on the Cancer Genome Atlas data mining. *Front Genet*. 2021;11:600248. doi:10.3389/fgene.2020.600248
24. Li H, Zou T, Meng S, Peng Y, Yang J. p21 protects cardiomyocytes against ischemia–reperfusion injury by inhibiting oxidative stress. *Mol Med Rep*. 2018;17(3):4665–4671. doi:10.3892/mmr.2018.8382
25. Huang S, Xu M, Liu L, et al. Autophagy is involved in the protective effect of p21 on LPS-induced cardiac dysfunction. *Cell Death Dis*. 2020;11(7):554. doi:10.1038/s41419-020-02765-7
26. Zeng ZM, Du HY, Xiong L, et al. BRCA1 protects cardiac microvascular endothelial cells against irradiation by regulating p21-mediated cell cycle arrest. *Life Sci*. 2020;244:117342. doi:10.1016/j.lfs.2020.117342
27. Bian R, Zhang L, Li D, Xu X. CDKN1A as a target of senescence in heart failure: Insights from a multiomics study. *Front Pharmacol*. 2024; 15:1446300. doi:10.3389/fphar.2024.1446300
28. Jha RK, Kouzine F, Levens D. MYC function and regulation in physiological perspective. *Front Cell Dev Biol*. 2023;11:1268275. doi:10.3389/fcell.2023.1268275
29. Li J, Wang H, Chen L, Zhong J, Wang J, Xiao J. Ischemia–reperfusion injury in human AC16 cardiomyocytes is modulated by AXIN1 depending on c-Myc regulation. *Ann Med Surg (Lond)*. 2023;85(10): 4844–4850. doi:10.1097/MS9.0000000000001139
30. Wolfram JA, Lesnefsky EJ, Hoit BD, Smith MA, Lee HG. Therapeutic potential of c-Myc inhibition in the treatment of hypertrophic cardiomyopathy. *Ther Adv Chronic Dis*. 2011;2(2):133–144. doi:10.1177/2040622310393059
31. Bello Roufai M, Li H, Sun Z. Heart-specific inhibition of protooncogene c-myc attenuates cold-induced cardiac hypertrophy. *Gene Ther*. 2007;14(19):1406–1416. doi:10.1038/sj.gt.3302995
32. Liu F, Wang Q, Ye H, et al. Identification of STAT3 and MYC as critical ferroptosis-related biomarkers in septic cardiomyopathy: A bioinformatics and experimental study. *J Mol Med*. 2025;103(1):87–100. doi:10.1007/s00109-024-02502-z
33. Zhang J, Wang J, Wu Y, Li W, Gong K, Zhao P. Identification of SLED1 as a potential predictive biomarker and therapeutic target of post-infarct heart failure by bioinformatics analyses. *Int Heart J*. 2021; 62(1):23–32. doi:10.1536/ihj.20-439
34. Wei Z, Yang Y, Li Q, et al. The transcriptome of circulating cells indicates potential biomarkers and therapeutic targets in the course of hypertension-related myocardial infarction. *Genes Dis*. 2021;8(4):555–568. doi:10.1016/j.gendis.2020.01.007
35. Wen C, Lan M, Tan X, et al. GSK3 β exacerbates myocardial ischemia/reperfusion injury by inhibiting Myc. *Oxid Med Cell Longev*. 2022; 2022(1):2588891. doi:10.1155/2022/2588891
36. Ji YR, Kim MO, Kim SH, et al. Effects of regulator of G protein signaling 19 (RGS19) on heart development and function. *J Biol Chem*. 2010;285(37):28627–28634. doi:10.1074/jbc.M109.073718
37. Wang Q, Traynor JR. Modulation of μ-opioid receptor signaling by RGS19 in SH-SY5Y cells. *Mol Pharmacol*. 2013;83(2):512–520. doi:10.1124/mol.112.081992
38. Ke S, Lu S, Xu Y, et al. RGS19 activates the MYH9/β-catenin/c-Myc positive feedback loop in hepatocellular carcinoma. *Exp Mol Med*. 2024;56(6):1412–1425. doi:10.1038/s12276-024-01244-9
39. Tian H, Zhao X, Zhang Y, Xia Z. Abnormalities of glucose and lipid metabolism in myocardial ischemia–reperfusion injury. *Biomed Pharmacother*. 2023;163:114827. doi:10.1016/j.biopha.2023.114827
40. Li D, Gao S. The interplay between T lymphocytes and macrophages in myocardial ischemia/reperfusion injury. *Mol Cell Biochem*. 2024; 479(8):1925–1936. doi:10.1007/s11010-023-04822-z
41. Horckmans M, Ring L, Duchene J, et al. Neutrophils orchestrate post-myocardial infarction healing by polarizing macrophages towards a reparative phenotype. *Eur Heart J*. 2016;38(3):187–197. doi:10.1093/eurheartj/ehw002
42. Zhuang Q, Li M, Hu D, Li J. Recent advances in potential targets for myocardial ischemia–reperfusion injury: Role of macrophages. *Mol Immunol*. 2024;169:1–9. PMID:38447462.
43. Magalhaes-Novais S, Blecha J, Naraine R, et al. Mitochondrial respiration supports autophagy to provide stress resistance during quiescence. *Autophagy*. 2022;18(10):2409–2426. doi:10.1080/15548627.2022.2038898
44. Yang J, Zhou R, Ma Z. Autophagy and energy metabolism. *Adv Exp Med Biol*. 2019;1206:329–357. doi:10.1007/978-981-15-0602-4_16